ORGANIC PROCESS RESEARCH & DEVELOPMENT
OPR&D



pubs.acs.org/OPRD
Article

# Modeling and Safe Operation of Fatty Alcohol Ethoxylation in a Continuous Flow Calorimeter

This Zahnd, Benedikt Brönnimann, Luca Moschen, Corina Constantin, Marlies Moser, Finn L. Steinemann, Alain G. Georg, Roland Borner, and Andreas Zogg*

Cite This: https://doi.org/10.1021/acs.oprd.5c00362



**ABSTRACT:** A safe, continuous process for the base-catalyzed ethoxylation of fatty alcohols at the miniplant scale is developed in this work. A flow process model based on preexisting semibatch and literature data is used to design a Fluitec flow calorimeter miniplant. Validation experiments at 1.5 mol equiv (mequiv) of ethylene oxide (EO) agreed well with semibatch kinetics, while 3 mequiv experiments showed considerable discrepancies. Critically, observed temperature peaks increased at higher flow rates, while the model predicts the opposite behavior. Caloric measurements using 1.5 mequiv of EO resulted in an average reaction enthalpy of 88 ± 4 kJ/mol ethylene oxide, which is in good agreement with the literature. A conservative total-failure scenario model predicted maximum temperature rises of 60 K (1.5 mequiv) and 104 K (3 mequiv), whereas experimental values were significantly lower (22 and 38 K). This article shows how simulations and theoretical calculations should guide practical experimental work and vice versa. Moreover, it demonstrates the feasibility of transferring semibatch data to continuous flow systems and emphasizes the importance of model validation under flow conditions.

**KEYWORDS:** *continuous flow calorimetry, ethoxylation, process modeling, process transfer*



## 1. INTRODUCTION

Fatty alcohol ethoxylates are nonionic surfactants that are often used in detergents, cosmetics, as well as pharmaceuticals. They are produced by dosing ethylene oxide (EO) to a fatty alcohol using homogeneous catalysts, typically NaOH or KOH.[1] EO is continuously added until the desired grade of ethoxylation is reached.

Industrial ethoxylation of fatty alcohols is mostly done in semibatch stirred tank reactors or venturi loop reactors (Buss reactor).[2] In either design, EO is present in the gas or liquid phase. Rapid explosive decomposition of gaseous EO can occur even if no oxygen is present.[3] Furthermore, EO can accumulate in the liquid phase and result in a runaway reaction in case the cooling of the reaction mass fails. Even though the challenges of working with EO are well-documented, serious accidents still occur regularly.[4−7]

Switching the process from semibatch to flow enables process intensification and improved safety for ethoxylation plants. A flow reactor can be feasibly operated at higher pressure and therefore avoids EO vapors inside the reactor. Higher temperatures and concentrations are also possible, which reduce reaction times and therefore the required active reactor volume for the same productivity.[8] The release of the reaction heat in a shorter time can be handled due to the considerably increased surface-to-volume ratio available for heat exchange.[9] In the future, flow ethoxylation may even enable the development and use of EO generators. Such generators would drastically reduce the amount of EO stored in ethoxylation plants and in transportation.[10]

The design of a safe process relies on an accurate thermochemical and kinetic description of the system, which can be obtained by reaction calorimetry. However, standard batch calorimeters are often not able to handle the extreme conditions and short reaction times possible in flow. As a result, flow calorimeters have been developed to obtain the required data for further process development and scale-up under flow conditions.[11] A challenge is the initial definition of process parameters for the safe operation of a flow calorimeter. Typically, there are no flow process data available. However, a (semi)batch process is already available as a basis for safety calculations. That is also the case for the fatty alcohol ethoxylation investigated in this work. The transfer of the batch process into a safe flow miniplant and the importance of model validation under flow conditions are demonstrated.

In this work, an existing commercial-scale semibatch process for the KOH-catalyzed ethoxylation of dodecanol (Scheme 1) is transferred to a Fluitec flow calorimeter (FFC) miniplant. First, a flow process model based on available process and

**Scheme 1. General Reaction Scheme of the KOH Catalyzed Ethoxylation of Alcohol**

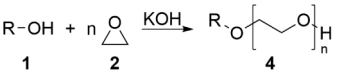


Received: September 25, 2025
Revised: January 29, 2026
Accepted: February 5, 2026

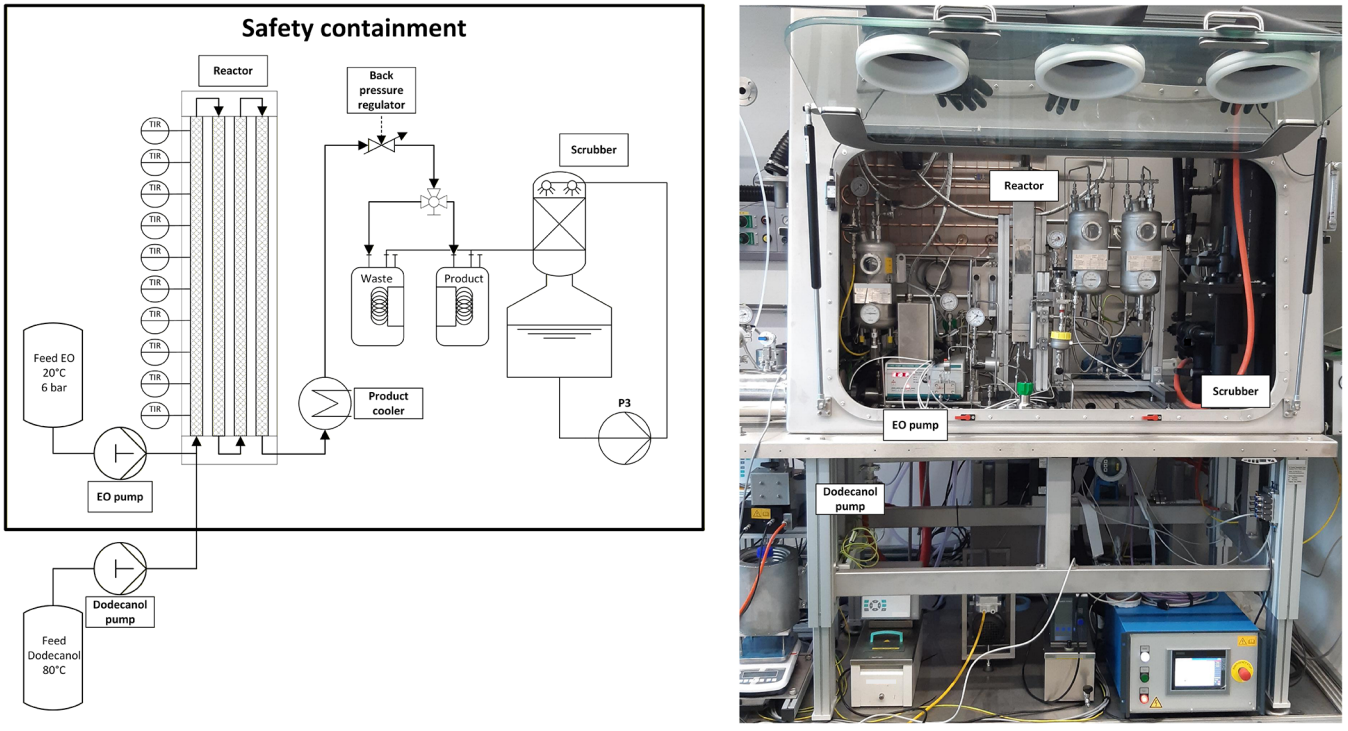


**Figure 1.** Process flow diagram and picture of the FFC miniplant used in this work. During operation, the glass front is closed, and the inside is inertized with nitrogen to prevent an explosive atmosphere.

literature data is established and used to design the miniplant. The model is refined and validated using newly obtained flow data.

## 2. MATERIALS AND METHODS

### 2.1. DSC

DSC measurements were performed using a Mettler Toledo DSC 3+ and evaluated using the STARe-Excellence software. 100 $\mu$L gold-plated, screwable, high-pressure crucibles, type BFT 94 by Bächler Feintech AG, were used for all measurements. The measurements were used to investigate whether any safety-relevant decompositions are present and to obtain an impression about reaction kinetics. Measurements of the reaction mass were performed by preparing a dried mixture of dodecanol and potassium hydroxide in the crucible and cooling with dry ice. The very volatile EO was then added under nitrogen atmosphere to the cooled crucible, which was then immediately closed.

### 2.2. Semi-Batch

Semi-batch experiments were performed in a 5L premex pressure reactor. The reactor was charged with dodecanol and 0.2−0.3 wt % potassium hydroxide, and the solution was dried under vacuum. After the reaction mass was brought to the reaction temperature, EO was dosed until the desired ethoxylation grade was reached.

### 2.3. Explosion Reactor

A high-pressure premex autoclave type HPM-P with a pressure rating of 300 bar was used for explosion pressure measurements (as previously published by Leonhardt et al.[12]), full-batch experiments, and vapor−liquid equilibrium measurements. For explosion pressure measurements, the desired mixture was charged into the reactor and heated to 30 °C. The mixture was stirred vigorously to simulate aerosol formation. Then, a 200 W BERU GN857 glow plug was used to ignite the vapor phase. The pressure was recorded using a Kistler 603C piezoelectric pressure sensor.

Experimental vapor pressure curves were obtained by charging the explosion reactor with uncatalyzed dodecanol and EO followed by slowly heating the reactor jacket. Vapor pressure curves of mixtures containing 1.5 and 3 mol equiv (mequiv) EO have been recorded at different heating ramps. The obtained curves were not published in this article due to confidentiality.

### 2.4. Flow Calorimeter

A flow calorimeter miniplant was built and used for model validation in this work. The miniplant was operated in an inert safety containment to prevent EO exposure and the formation of an explosive atmosphere in the laboratory around the reactor. All wetted metals were either 1.4404 or 1.4571 to avoid incompatible metals.[13] A process flow diagram (PFD) and a picture of the miniplant are shown in Figure 1. A Fluitec Contiplant consisting of four 0.5 m long reactors with an inner diameter of 7.8 mm in series, equipped with stainless steel CSE-X static mixers, was used. The first of the reactors was equipped with an axial 10-point temperature sensor to obtain temperature profiles and was used as a Fluitec flow calorimeter (FFC). The purpose of the other reactors was to ensure full EO conversion, and they were not modeled. The total volumetric flow rate through the reactors ranged from 3 to 8 mL/min, which corresponds to typical mixing times of 4.5 to 1.5 s according to the manufacturer. The residence times ranged from 5.67 to 2.13 min per reactor. EO and dodecanol were both fed by Bischoff Multitherm 200 Model 3351 pumps, where the dodecanol line was heated to prevent clogging. The reaction mass was cooled after exiting the last reactor. Finally, the reaction mass was released after the back pressure regulator and collected in two receiver tanks. The reaction mass was purged with a continuous nitrogen flow to remove unreacted EO. A scrubber operated with a 5 wt % phosphoric acid solution was used to remove and destroy any EO in the purge gas flow. Calorimetric evaluation was performed using the Fluitec milli-scale reaction calorimeter calculation tool V 3.04, which calculates the reaction enthalpies according to Steinemann et al.[14]

## 3. MODEL BASIS

The available semibatch data and literature are used as a basis to establish a semibatch model of the investigated ethoxylation, which is validated against experimental pressure curves. The model is adapted into a flow process model and used to find


https://doi.org/10.1021/acs.oprd.5c00362
Org. Process Res. Dev. XXXX, XXX, XXX−XXX

**Scheme 2. Reaction Mechanism of the Alkoxylation According to Santacesaria et al.[2]**

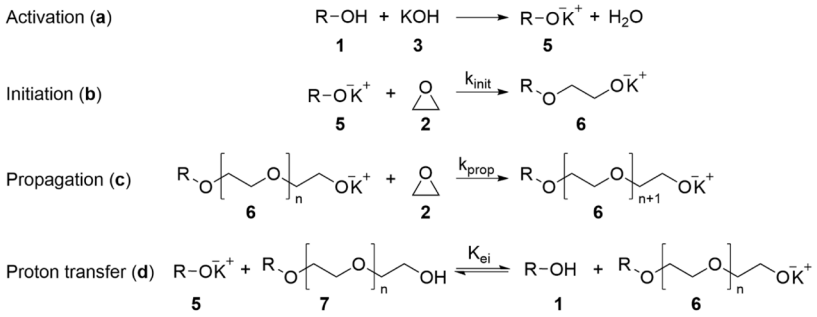


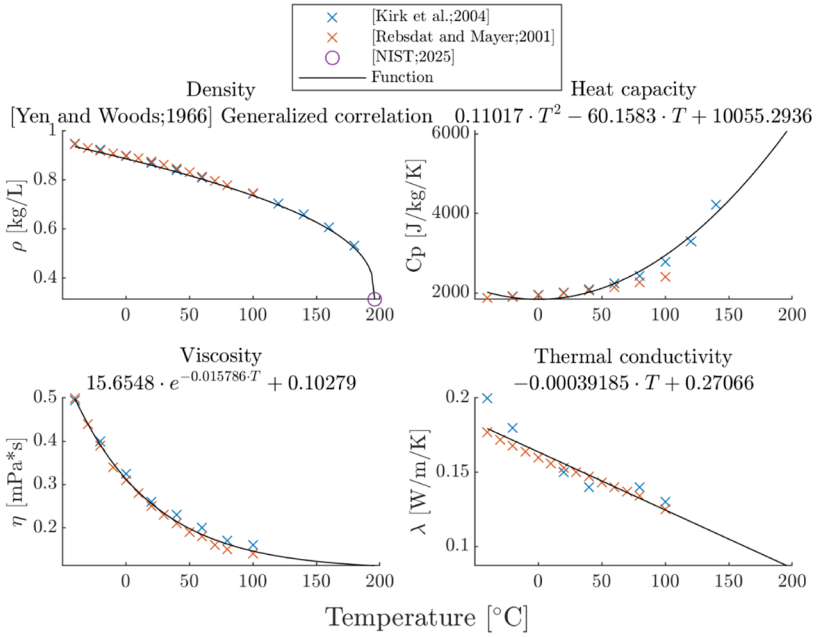


**Figure 2.** Comparison of functions of temperature-dependent physical properties in the range of −40 to 200 °C of pure liquid EO and literature data collected by Dever et al.[22] and Rebsdat and Mayer.[23] Density is obtained from a generalized correlation by Yen and Woods,[21] while heat capacity, viscosity, and thermal conductivity are calculated using eqs 5, 6, and 7 fitted in this work, respectively.

safe process conditions (see Chapter 4.5). With additional information regarding the thermal stability by DSC and explosion measurements, a safe process and corresponding operating ranges are defined based on a risk analysis.[15]

### 3.1. Reaction Mechanisms and Kinetics

The commercial synthesis of polyethoxylated fatty alcohols is typically performed using a strong base as a catalyst.[16] Scheme 2 shows the reaction mechanism of the ethoxylation according to Santacesaria et al.[2] Activation of the fatty alcohol by deprotonation occurs before EO dosing is started, and the formed water is removed by drying at elevated temperature and low pressure. The activated fatty alcohol reacts with EO in the liquid phase to form the first ethoxylate, which may react with additional EO by propagation reaction. Finally, there is a proton transfer equilibrium between the starter and ethoxylates.

By assuming that the kinetics of the propagation reaction are independent of chain length, the reaction model can be simplified. The corresponding rate expressions for the initiation and propagation reactions are given by eqs 1 and 2, respectively,

$$r_{\text{init}} = k_{\text{init}} \times [\text{EO}] \times [\text{RO}^{-}\text{K}^{+}] \tag{1}$$

$$r_{\text{prop}} = k_{\text{prop}} \times [\text{EO}] \times [\text{RO(EO)}_i^{-}\text{K}^{+}] \tag{2}$$

where the concentrations of activated fatty alcohol $[\text{RO}^{-}\text{K}^{+}]$ and the total ethoxylate concentration $[\text{RO(EO)}_i^{-}\text{K}^{+}]$ are calculated by eqs 3 and 4.[17] The required kinetic and equilibrium constants were taken from literature.[18]

$$[\text{RO}^{-}\text{K}^{+}] = \frac{[\text{ROH}] \times [\text{KOH}]^{\text{total}}}{[\text{ROH}] + K_{\text{ei}} \times [\text{RO(EO)}_j\text{H}]} \tag{3}$$

$$[\text{RO(EO)}_j^{-}\text{K}^{+}] = K_{\text{ei}} \times [\text{RO}^{-}\text{K}^{+}] \times \frac{[\text{RO(EO)}_j\text{H}]}{[\text{ROH}]} \tag{4}$$

### 3.2. Vapor–Liquid Equilibrium

The vapor–liquid equilibrium (VLE) of EO in ethoxylate is required to calculate the concentration of liquid-dissolved ethylene oxide [EO] available for the reaction. EO solubility for the semibatch process is described using Wilson equations and parameters described by Santacesaria et al.[2] It should be noted that these empirical parameters are not valid for the high EO concentrations and temperatures possible in a continuous process.



https://doi.org/10.1021/acs.oprd.5c00362
Org. Process Res. Dev. XXXX, XXX, XXX−XXX

### 3.3. Physical Properties

In this work, mixing rules according to the VDI Heat Atlas[19] are used to obtain the various required liquid phase properties from pure liquid EO and ethoxylated fatty alcohol properties. The density of ethoxylated dodecanol is obtained by an expression published by Di Serio et al.,[20] while EO density is estimated by the Yen and Woods correlation.[21] Correlations for ethoxylate heat capacity and viscosity are taken from Amaral and Giudici.[17] Functions for liquid EO specific heat capacity (eq 5), viscosity (eq 6), and thermal conductivity (eq 7) were fitted using data collected by Dever et al.[22] and Rebsdat and Mayer.[23]

$$\mathrm{cp}_{\mathrm{EO},L}\left[\frac{\mathrm{J}}{\mathrm{kg}\times\mathrm{K}}\right] = 0.11017\times T^2 - 60.153\times T + 10055.2936 \tag{5}$$

$$\eta_{\mathrm{EO},L}[\mathrm{Pa}\times\mathrm{s}] = 15.9548\times e^{-0.015786\times T} + 0.10279 \tag{6}$$

$$\lambda_{\mathrm{EO},L}\left[\frac{\mathrm{W}}{\mathrm{m}\times\mathrm{K}}\right] = -0.00039185\times T + 0.27066 \tag{7}$$

The temperature dependent functions and the corresponding data used to fit the functions are listed in Figure 2. The temperature range for heat capacity data was −40 to 150 °C and for viscosity and thermal conductivity data −40 to 100 °C. Process temperatures up to 200 °C way beyond these ranges require considerable extrapolation and should be done with caution. However, extrapolation of the correlations proposed in this work shows reasonable behavior up to 200 °C. Further details on the calculations of the physical properties are given in the Supporting Information.

### 3.4. Flow Reactor Modeling

Modeling of the flow reactor is performed using a tanks-in-series model according to Levenspiel.[24] Here, the flow reactor is modeled as a number of the same-sized cascading continuously stirred reactors (CSTRs). The number of CSTRs to model a given flow reactor can be obtained from experimental Bodenstein numbers derived from residence time distributions.[25] The CSE-X static mixer used in this work was modeled as 50 CSTRs in series, with each segment having the same volume. Figure 3 shows the heat and molar flows considered for each reactor segment.

The mass balance equation of a component "$i$" for a reactor segment "R" is the sum of the molar flow in $F_{\mathrm{in}}$ from the previous reactor segment (eq 8), the molar flow out $F_{\mathrm{out}}$ to the next reactor segment (eq 9), and the reaction occurring $F_{\mathrm{rx}}$ in the given reactor segment (eq 10),

$$F_{\mathrm{in},i,\mathrm{R}} = \frac{\dot{V}_{\mathrm{in}}\times\rho_{\mathrm{R}}}{M_{i,\mathrm{R}}}\times w_{i,\mathrm{R}-1} \tag{8}$$

$$F_{\mathrm{out},i,\mathrm{R}} = \frac{\dot{V}_{\mathrm{in}}\times\rho_{\mathrm{R}}}{M_{i,\mathrm{R}}}\times w_{i,\mathrm{R}} \tag{9}$$

$$F_{\mathrm{rx},i,\mathrm{R}} = (r_{\mathrm{init,R}}\times\nu_{\mathrm{init},i} + r_{\mathrm{prop,R}}\times\nu_{\mathrm{prop},i})\times V_{\mathrm{RM,R}} \tag{10}$$

Here, $\dot{V}$ is the volumetric flow of the reaction mass, $M$ is the molar mass, $w$ is the mass fraction, $\nu$ is the stoichiometric coefficient, and $V$ is the volume of the segment. The total mass balance equation is given in eq 11 as the sum of the above molar flows,

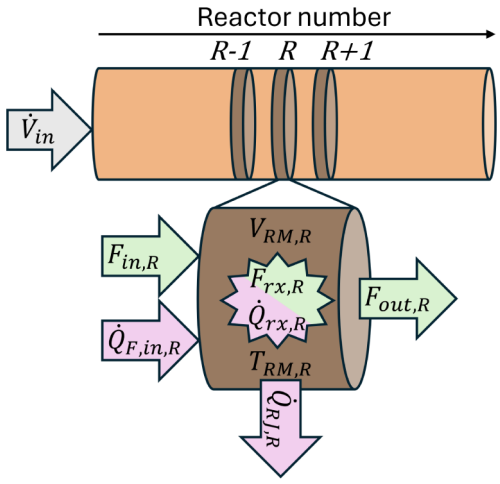


**Figure 3.** Tanks-in-series model for a flow reactor, including the molar flow contributions in green and heat flow contributions in violet. $V_{\mathrm{RM,R}}$ is the volume, and $T_{\mathrm{RM,R}}$ is the temperature of reactor segment "R". $F_{\mathrm{in}}$ is the molar flow from the previous reactor segment, and $F_{\mathrm{out}}$ is the molar flow into the next reactor segment. $F_{\mathrm{rx,R}}$ is the molar flow due to the reaction in the segment, with $\dot{Q}_{\mathrm{rx,R}}$ being the associated heat flow. $\dot{Q}_{F,\mathrm{in,R}}$ is the heat flow due to reaction mass entering from the previous segment, and $\dot{Q}_{\mathrm{RJ,R}}$ is the heat flow to the reactor jacket. $\dot{V}_{\mathrm{in}}$ is the total educt volume flow into the reactor.

$$\frac{\mathrm{d}n_{i,\mathrm{R}}}{\mathrm{d}t} = F_{\mathrm{in},i,\mathrm{R}} - F_{\mathrm{out},i,\mathrm{R}} + F_{\mathrm{rx},i,\mathrm{R}} \tag{11}$$

To keep the mass balance consistent, we must further consider the changing average molar mass of the polymer. This is done by first calculating the total mass of the polymer in each reactor segment by the mass balance equation given (eq 12). The mean polymer molar mass $M_{7,\mathrm{R}}$ can then easily be obtained from the total polymer mass $m_{7,\mathrm{R}}$ and moles $n_{7,\mathrm{R}}$.

$$\frac{\mathrm{d}m_{7,\mathrm{R}}}{\mathrm{d}t} = F_{\mathrm{in},7,\mathrm{R}}\times M_{7,\mathrm{R}-1} - F_{\mathrm{out},i,\mathrm{R}}\times M_{7,\mathrm{R}} + V_{\mathrm{RM,R}}\times(r_{\mathrm{init,R}}\times(M_1 + M_2) + r_{\mathrm{prop,R}}\times M_2) \tag{12}$$

The heat balance equation considers three heat flows. Similar to the mass flow equations, the heat flow from the previous reactor segment $\dot{Q}_{F,\mathrm{in}}$ (eq 13) and the heat flow due to the chemical reaction (eq 14) are considered,

$$\dot{Q}_{F,\mathrm{in,R}} = \mathrm{cp}_{\mathrm{R}-1}\times\dot{m}\times(T_{\mathrm{RM,R}-1} - T_{\mathrm{RM,R}}) \tag{13}$$

$$\dot{Q}_{\mathrm{rx,R}} = (-r_{\mathrm{init,R}}\times\Delta_{\mathrm{R}}H_{\mathrm{init}} - r_{\mathrm{prop,R}}\times\Delta_{\mathrm{R}}H_{\mathrm{prop}})\times V_{\mathrm{RM,R}} \tag{14}$$

where $\Delta_{\mathrm{R}}H_{\mathrm{init}}$ and $\Delta_{\mathrm{R}}H_{\mathrm{prop}}$ are the enthalpies of reaction of the initiation and propagation reactions, respectively. In this work, both reactions are assumed to yield the same enthalpy, which is dominated by the ring opening of EO, releasing 92 kJ/mol.[26] The final contribution to the heat balance is the heat flow between the reaction mass and the jacket fluid $\dot{Q}_{\mathrm{RJ}}$ given in eq 15.

$$\dot{Q}_{\mathrm{RJ,R}} = k_{\mathrm{RJ,R}}\times A_{\mathrm{RJ,R}}\times(T_{\mathrm{RM,R}} - T_{\mathrm{J,R}}) \tag{15}$$

where $A_{\mathrm{RJ,R}}$ is the heat exchange area and $k_{\mathrm{RJ,R}}$ is the total heat exchange coefficient between the reaction mass and the jacket fluid for a given segment "R" according to correlations


https://doi.org/10.1021/acs.oprd.5c00362
Org. Process Res. Dev. XXXX, XXX, XXX−XXX

described by Moser et al.[27] Further details on the calculation of the total heat exchange coefficient are given in the Supporting Information. The heat balance equation for a reactor segment is given in eq 16,

$$\frac{dT_{RM,R}}{dt} = \frac{\dot{Q}_{F,in,R} + \dot{Q}_{rx,R} - \dot{Q}_{RJ,R}}{m_{RM,R} \times cp_R} \quad (16)$$

Finally, the heat balance of the jacket fluid is calculated by eq 17 as the sum of the heat flow from the reaction mass $\dot{Q}_{RJ,R}$ and the heat flow due to new fluid entering the segment,

$$\frac{dT_{J,R}}{dt} = \frac{\dot{Q}_{RJ,R} + \dot{m}_{J,R} \times cp_J \times (T_{J,R-1} - T_{J,R})}{m_{J,R} \times cp_J} \quad (17)$$

## 4. RESULTS AND DISCUSSION

Different experimental methods as well as literature are used to establish a reactor model for flow ethoxylation. Designing a safe miniplant for ethoxylation was performed based on flow reactor model calculations. During the risk assessment process, different designs and conditions were evaluated in silico to establish a lab-scale flow ethoxylation miniplant. As most of the model components are based on measurements not performed in flow, verification of the model under flow conditions must be performed before further scale-up.

### 4.1. DSC

Various DSC measurements have been performed. Pure EO decomposition was observed to start at around 400 °C, which agrees with temperature ranges found literature.[28,29] Produced ethoxylates were also investigated for decomposition, but no notable thermal signals were observed in the investigated temperature range of up to 470 °C. Consequently, no measures to handle safety-relevant thermal decomposition reactions had to be defined during the risk analysis. Measurements of the reaction mass show elevated total ethoxylation heat of reaction; 103.8 kJ/mol of EO was obtained, while a literature value of 92 kJ/mol was used in this work.[23,26] We attribute this difference to two main effects. First, considerable changes of the heat capacity of the reaction mass during the reaction result in an inaccurate baseline. Second, the EO vapor in the crucible condenses as the reaction progresses, releasing additional heat that cannot be distinguished from the reaction heat. As we will discuss later, Chapter 4.4, we found that available VLEs are not applicable under these conditions. As a result, the exact quantification of this effect is not possible. However, a rough estimate at the observed start of the reaction (200 °C) using Raoult's law results in a total additional heat release due to condensation of ~20 kJ/mol total EO. While this approximation must be clearly understood as a very rough calculation, it shows the described effect to be of the correct order of magnitude to explain the observed differences.

In Figure 4, the experimental and simulated heat flow curves from the kinetic model[18] adapted in this work are overlaid. It can be clearly shown that the kinetics observed in DSC do not agree with the literature kinetics. It should be noted that the model assumes no vapor phase, so the previously discussed EO condensation is not considered. That, and the lack of mixing in the crucible of the DSC, could very well be the underlying reason for the observed differences.

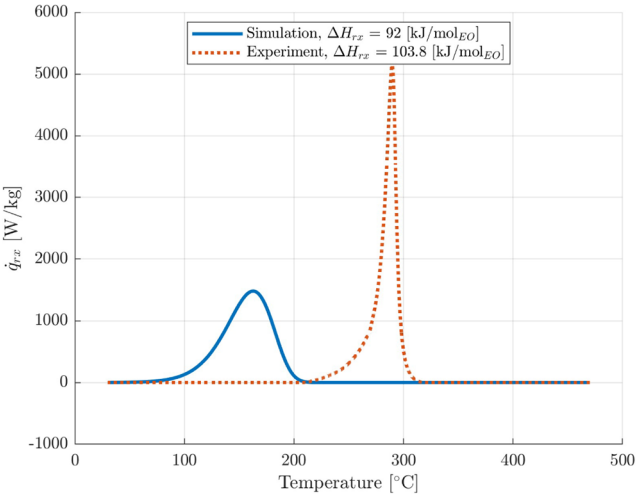


**Figure 4.** Specific reaction power curves obtained from DSC (dotted orange line) and by simulation using the kinetic model established by Amaral and Giudici,[17] adapted in this work (solid blue line). Four mg dodecanol with 0.25 wt % KOH and 5.6 mg EO were used for the measurement. The crucible was loaded under nitrogen, and a dynamic heating rate of 4 K/min was used.

### 4.2. Semi-Batch

The current semibatch process was performed to validate the kinetic model. Reaction mass temperature is imposed for the simulation, as modeling the heat transfer in the semibatch vessel was not relevant. Furthermore, it was assumed that the reaction is not mass transfer controlled and that the phases are always at equilibrium. Figure 5 shows the experimental and simulated pressure curves. Simulation using the VLE model by Santacesaria et al.[2] and the kinetic model by Amaral and Giudici[18] predicts consistently higher pressures than those experimentally observed. Good agreement of the model

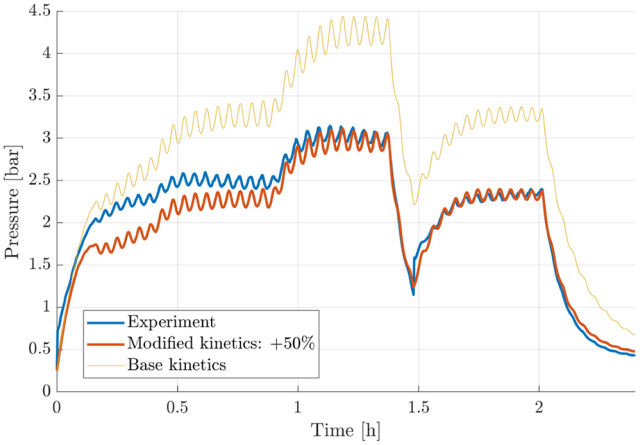


**Figure 5.** Experimental (blue curve) and simulated pressure curves (base model yellow curve; modified model orange curve) of the semibatch process for an average of 6 EO units per ethoxylate. These data were previously presented at the Pharma Forum 2024.[30] The dosing rate of EO and liquid temperature are imposed on the simulation. The base kinetic model established by Amaral and Giudici[18] was found to result in higher pressures than observed. Increasing the reaction rate of both the initiation (eq 1) and the propagation reaction (eq 2) by 50% found good agreement. The pressure drop around 1.3 h is due to a short interruption of EO feed to depressurize the feed vessel.


https://doi.org/10.1021/acs.oprd.5c00362
Org. Process Res. Dev. XXXX, XXX, XXX−XXX

prediction can be achieved by increasing the reaction rate of both the initiation reaction (eq 1) and the propagation reaction (eq 2) by 50%. It should be noted that the data set used to fit the empirical VLE contains only limited data at the reaction temperature of 150 °C.[20] Additionally, significantly higher liquid EO molar fractions and temperatures can be achieved in a flow process. Validation of the VLE at flow process conditions must be performed.

### 4.3. Explosion Reactor

During the risk assessment, it was noted that there is an explosion risk in the product tank in case unconverted reaction mass would leave the reactor that contains high amounts of EO. As the reaction mass passes through the back pressure regulator, unreacted EO could potentially form vapors and aerosols, which can result in a potentially explosive atmosphere even in an inertized tank. Explosion pressures of 12 times the starting pressure can be expected, even more if liquid EO is present.[31] Literature also reports very high explosion when EO mist is present.[32] As the formation of a mist due to the sudden depressurization of the reaction mass is plausible and due to the lack of literature data under such conditions, the potential explosion pressures were further investigated under agitated conditions.

Before performing experiments, expected explosion pressures are calculated to ensure the reactor will hold. Different decomposition products have been observed in the literature. In this work, full decomposition into methane and carbon monoxide is assumed, as this decomposition releases the most energy.[33] As liquid phase decomposition of EO is only reported under extreme conditions[34] not relevant to the scenario in this work, only vapor phase decomposition is considered. The required thermodynamic values and parameters for EO, methane, and carbon monoxide are obtained from the NIST Chemistry WebBook.[35−37] Further details on the calculation of the explosion pressure are given in the Supporting Information.

The calculated and measured explosion pressures are listed in Figure 6. The calculated pressures are consistently higher than the measurements, indicating that no considerable liquid phase decomposition is triggered. Due to the small size of the explosion reactor (125 mL), not the full adiabatic explosion pressure can be measured (see also Leonhardt et al.[12]). As a consequence of these measurements and calculations, the receiver vessels for the reaction mass were designed to be pressure proof up to 20 bar. The authors strongly recommend reassessing these explosion measurements for a potential scale-up to production scale. So far, these data only ensure the safe operation of the FFC plant described within this publication.

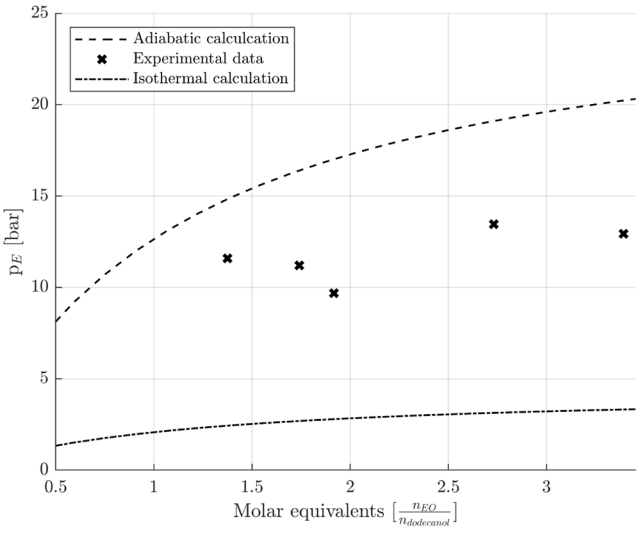


**Figure 6.** Calculated adiabatic (dashed line) and isothermal explosion pressure (dashed−dotted line), as well as measured explosion pressures (x), for an initial temperature of 30 °C under agitated conditions as a function of EO mequiv in dodecanol.

### 4.4. VLE Verification

Based on the risk analysis, we concluded that the formation of a gaseous phase in the flow reactor is to be avoided as that would lead to unpredictable process behavior and potentially explosive vapor phase inside of the reactor. As such, verification of the VLE is critical to calculate the expected vapor pressure of the reaction mass and the required back pressure regulator setting. Vapor pressures are recorded for an initial charge containing 3 and 1.5 mequiv of EO and uncatalyzed dodecanol. The obtained curves are not published in this work due to confidentiality.

The predictions of the Wilson and NRTL models by Di Serio et al.[20] (Wilson was used for semibatch simulations), Raoult's law, and the predictive Soave−Redlich−Kwong[38] equation of state are evaluated against the experimental vapor pressure curves. Large deviations at higher temperatures were found for all of the models. The parameters for the empirical Wilson and NRTL models were originally fitted for considerably lower EO concentrations. As such, the observed model inaccuracies were not surprising due to extrapolation well beyond the range of the original data. Rerunning the temperature program with the same reaction mass found no significant difference between the observed pressures. We can therefore conclude with relative confidence that no significant uncatalyzed reaction occurred during the vapor pressure measurements. Evidently, nonideal interactions between EO and dodecanol significantly affect the vapor pressure at elevated temperatures, which are not captured by the models investigated.

Considerable experimental effort is required to establish a new VLE model that is valid at flow reactor conditions, and to the best of the author's knowledge, no applicable data have been published in the literature. However, we only require the pressure calculation to define the required back pressure regulator setting to ensure no gas phase formation. As such, Raoult's law was used with a large safety factor of 50%. Further details on the calculations of VLE are given in the Supporting Information.

### 4.5. Definition of Safe Process Conditions

The initial model of the flow process is used to evaluate safe process conditions. In the first step, the critical process responses and their limits as well as the variable process parameters are defined. Simulation of the flow process at various parameter combinations enables parameter set exploration and the definition of suitable process conditions to perform the first set of validation experiments.

Normally, the maximal reaction mass temperature is critical to avoid triggering of undesired decomposition reactions of the liquid phase, leading to a thermal runaway. As stated above, the investigated ethoxylation process shows no decomposition of the product up to 470 °C by DSC, so a thermal runaway due to decomposition of the liquid phase is unlikely. However, the


https://doi.org/10.1021/acs.oprd.5c00362
Org. Process Res. Dev. XXXX, XXX, XXX−XXX

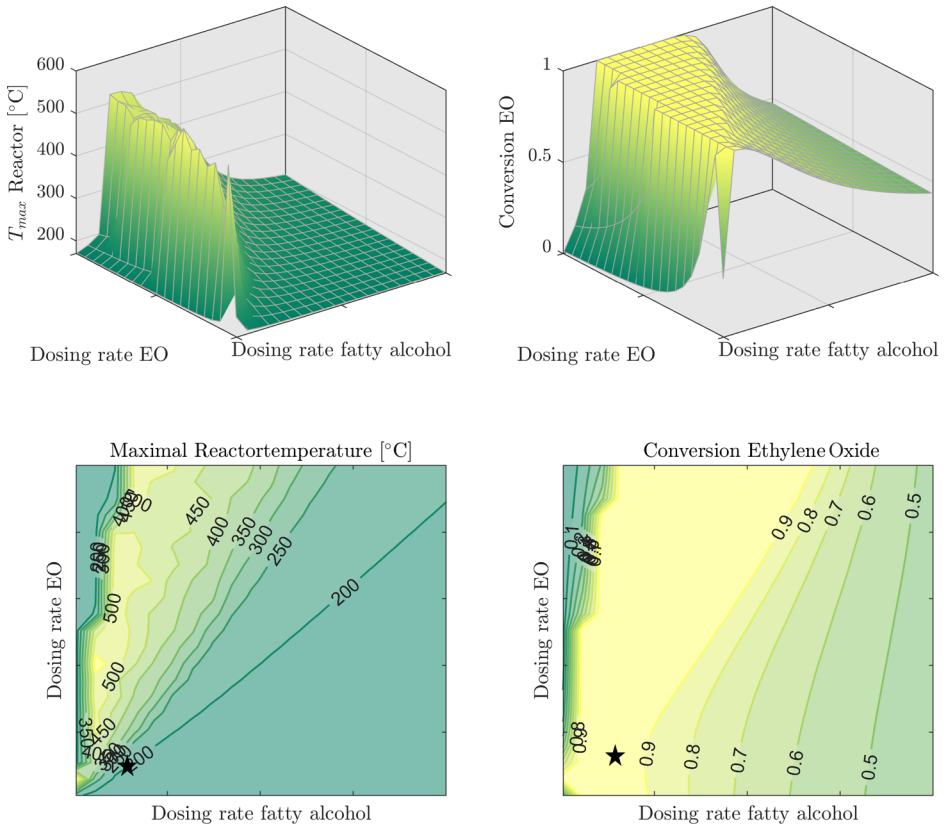


**Figure 7.** Response surface (top) and corresponding contour plot (bottom) of the maximal reactor temperature $T_{max}$ reactor (left) and EO conversion (right) for a jacket temperature of 170 °C for different EO and dodecanol dosing rates. The chosen feed rates (★) correspond to 1.5 mequiv of EO. These data were previously presented at the Pharma Forum 2024.[30]

formation of EO vapor, followed by gas phase decomposition, is critical. It was decided to limit the reaction mass temperature to 200 °C in order to not grossly exceed the critical temperature of EO of 195.8 °C[36] and due to material limits of the equipment.

The conversion of EO is critical to avoid excessive unreacted EO leaving the reactor, as that could lead to the formation of mist when the reaction mass passes through the back pressure regulator due to rapid evaporation. In the simulation, only the first of the four reactors in series is considered. As the model has not yet been validated, a minimum conversion of 90% of the EO in the first reactor was set to account for model inaccuracies.

The independent process parameters are the two educt feed flows and the reactor jacket temperature. Response surfaces of educt flows at different jacket temperatures are created and evaluated. Figure 7 shows the response surfaces and contour plots for a jacket temperature of 170 °C. The identified feed flows correspond to a total educt flow of 4 mL/min and 1.5 mequiv of EO. The adiabatic temperature rise $\Delta T_{ad}$ can be calculated using eq 18,

$$\Delta T_{ad} = \frac{\Delta_r H \times x_{EO}}{cp_{RM} \times \sum mw_i \times x_i} \quad (18)$$

where $x_{EO}$ is the liquid molar fraction of EO, $cp_{RM}$ is the heat capacity of the reaction mass, and mw*i* is the molar weight of the component "*i*". Assuming a constant conservative heat capacity $cp_{RM}$ of 3.0 kJ/kg/K, an adiabatic temperature rise of 182 K is obtained for 1.5 mequiv of EO.

As previously discussed, Raoult's law with a safety factor of 50% is used to estimate the EO vapor pressure in the flow reactor to find the back pressure regulator setting. Figure 8 shows the predicted pressure during the startup until steady state operation. The highest predicted pressure is 32.3 bar. Therefore, the back pressure regulator is set to 50 bar to ensure no EO vapors are formed in the reactor.

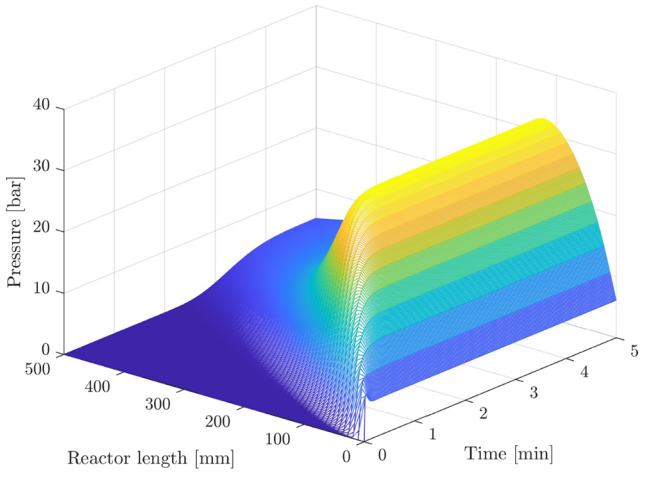


**Figure 8.** Plot of predicted vapor pressure by Raoult's law in the flow calorimeter during startup and in steady state operation at the process conditions obtained from Figure 7. The highest predicted pressure is 32.3 bar.



https://doi.org/10.1021/acs.oprd.5c00362
Org. Process Res. Dev. XXXX, XXX, XXX−XXX

### 4.6. Flow Reactor Model Validation

Data for flow reactor model validation are obtained at the previously defined safe process conditions. In Figure 9, the measured steady-state temperature profiles of two experimental runs are overlaid with model predictions. The modified kinetics obtained from semibatch experiments in this work do not match the experimental data and overestimate reaction rates. However, using the kinetics proposed by Amaral and Giudici[18] results in good agreement with experimental data. The temperature of the reaction mass at the first sensor was considerably higher than expected. The root cause of this observation is assumed to be due to the hot head plate and the premixer already heating up the reaction mass. The overall effect on critical safety relevant process parameters is, however, negligible. Manual adjustment of the inlet temperature showed no significant increase of the simulated temperature peak.

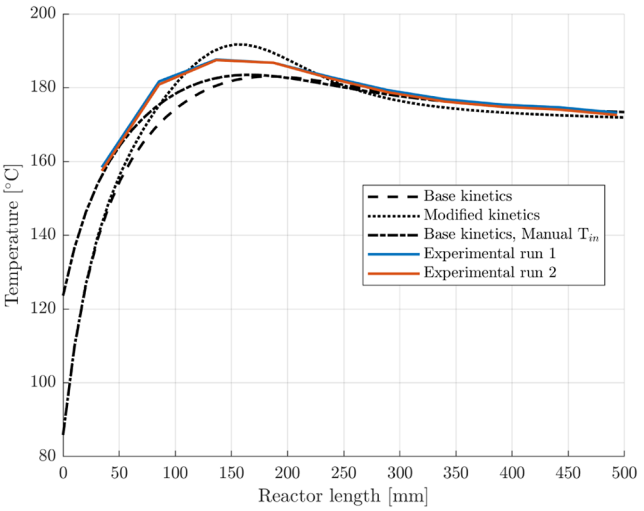


**Figure 9.** Experimental (solid lines) and simulated (dotted lines) temperature profiles of the flow reactor at steady state with 1.5 mequiv EO. The base kinetics[18] showed good agreement with the experimental data. Manually adjusting the inlet temperature to account for heat transfer in the head plate showed no significant increase in the maximal reactor temperature.

To further validate the model, a screening experiment was conducted. While the feed ratios were kept constant at 1.5 mequiv of EO, total feed flow from 3 to 8 mL/min and jacket temperatures from 160 to 170 °C were tested. Some combinations of high feed flow and low jacket temperatures were not performed, as low EO conversion was predicted. The measured and simulated temperature profiles are shown in Figure 10. Model predictions agree well with experimental data at lower flow >5 mL/min but show significant discrepancies at higher flow.

An important observation is that the observed temperature peak increases at higher flows. Figure 11 visualizes this well by overlaying the experimental temperature profiles at a 170 °C jacket temperature. This observation is opposite to the expected behavior and may imply additional relevant effects not considered so far. A possible explanation may be local mass transfer limitations that are minimized at higher flows and result in higher-than-expected local reaction rates. Certainly, further investigation into the observed phenomena is required before further scale-up is conducted.

The total reaction heats released for each of these operating conditions are given in Table 1. They are calculated according to methods by Steinemann et al.[14] using the Fluitec milli-scale reaction calorimeter calculation tool V 3.04. Measurements at

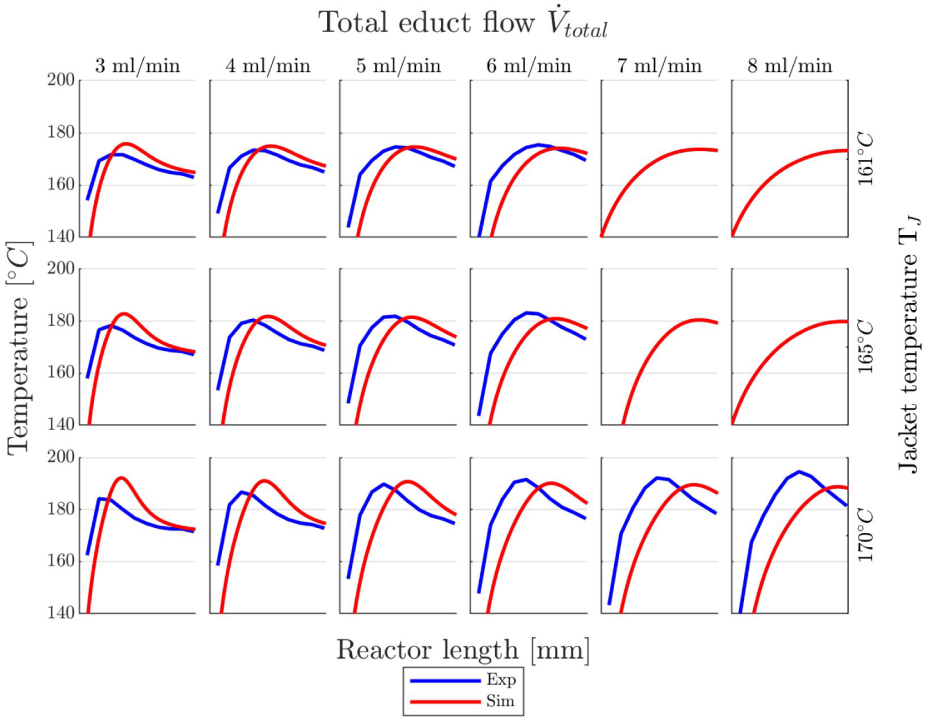


**Figure 10.** Measured (blue) and simulated (red) temperature profiles of screening experiments for 1.5 mequiv of EO. Jacket temperatures of 161, 165, and 170 °C and total educt flow rates of 3 to 8 mL/min are screened. Some high-flow and low-temperature experiments are not performed due to low predicted EO conversion.


https://doi.org/10.1021/acs.oprd.5c00362
Org. Process Res. Dev. XXXX, XXX, XXX−XXX

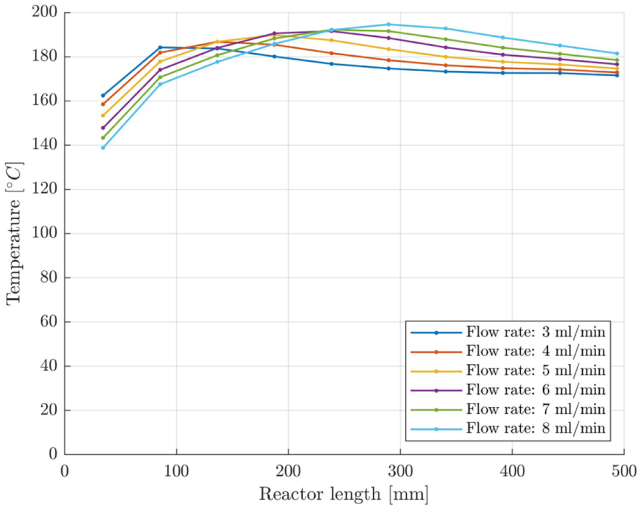


**Figure 11.** Overlay of steady-state temperature profiles from experiments with 1.5 mequiv of EO and a jacket temperature of 170 °C for different flow rates. Temperature peaks increase with higher flow rates.

**Table 1. Calculated Reaction Heats for the Ethoxylation of 1.5 Mequiv EO Experiments at Different Flows and Jacket Temperatures**

| Total feed flow (mL/min) | *T* Jacket (°C) | Reaction heat (kJ/mol EO) |
|---|---|---|
| 3 | 161 | −73[a] |
| | 165 | −74[a] |
| | 170 | −71[a] |
| 4 | 161 | −79[b] |
| | 165 | −86 |
| | 170 | −82 |
| 5 | 161 | −79[b] |
| | 165 | −86 |
| | 170 | −92 |
| 6 | 161 | −75[b] |
| | 165 | −86 |
| | 170 | −93 |
| 7 | 170 | −90 |
| 8 | 170 | −89 |

[a]Unreliable due to low flow. [b]Lower apparent enthalpy due to incomplete conversion.

3 mL/min total flow result in lower apparent reaction enthalpies due to the low flow rates. Similarly, measurements at 161 °C jacket temperature result in lower reaction enthalpies due to incomplete conversion of EO. All other measurements have an average reaction heat of −88.0 kJ/mol EO with a standard deviation of 4 kJ/mol, which is in good agreement with the literature. It should be noted that total conversion of EO in the first reactor segment with the axial temperature sensor cannot be assured. However, the good agreement between the obtained reaction heats at different flow rates and temperatures indicates that only insignificant amounts of EO were left after the calorimeter segment.

To further evaluate model limitations, an additional screening experiment for 3 mequiv of EO was conducted. Temperatures beyond the previously set limit of 200 °C were expected. Using eq 18 and assuming a constant conservative heat capacity of 3.0 kJ/kg/K, an adiabatic temperature rise of 288 K is obtained for 3 mequiv of EO. However, the potential consequences in case of equipment failure were considered an acceptable safety risk due to the small reactor volume and additional safety containment around the miniplant.

The measured and simulated temperature profiles for 3 mequiv of EO are shown in Figure 12. It is apparent that model predictions are inaccurate under these conditions. Here, significant temperature spikes to over 230 °C are observed, while model predictions stay below 200 °C. Critically, model predictions for maximal reactor temperature decrease as flow increases, while the opposite is observed in the experimental data. This is consistent with observations in 1.5 mequiv experiments.

Caloric evaluation of the steady state temperature curves requires an accurate description of the heat flow from the reaction mass to the jacket fluid. These correlations by Moser et al.[27] rely heavily on accurate liquid phase properties. The correlations for physical properties described in Chapter 3.3 already required considerable extrapolation for the 1.5 mequiv experiments. The considerably higher temperature peaks observed in the 3 mequiv experiments require even further extrapolation, introducing substantial uncertainty. Particularly, the Yen and Woods correlation[21] used for liquid EO density is problematic. It has no real solutions above the critical temperature (195.8 °C), and the value is fixed at the critical density in the simulation. The limited conditions of this data set that do not present high temperature in turn do not reach complete conversion in the calorimeter section of the reactor. As a result, the quantitative evaluation of the 3 mequiv data set using the current physical property correlations and experimental setup is deemed not viable.

Overall, the flow reactor model needs to be refined. It seems that reaction rates do not linearly increase with increasing EO concentration, which may indicate a higher reaction order at high concentrations. However, no reasonable reaction mechanism for such a behavior was found in this work. The model predicts lower temperature peaks with increased flows due to better heat transfer. Experimental data clearly show the opposite, indicating an effect which is not modeled yet. It should be noted that larger deviations in apparent reaction rates at higher temperatures were already noted in the original publication of the kinetic constants where the temperature range of the data was 130 to 180 °C.[17] Also discussed are potential gas−liquid mass transfer limitations at higher temperatures, which are not relevant in a flow process and may be the underlying reason that the reaction kinetics in flow are faster than what is observed in semi- and full-batch experiments. The concentration of liquid EO is also considerably higher in the flow process, which is a further error source. The assumption that reaction rates do not change with the chain length may also be incorrect. Especially in the temperature profiles for the 3 mequiv screening experiments (Figure 12), a delayed rate increase can be seen, which could indicate faster reaction rates for the propagation reaction compared to the initiation. Mixing effects, such as local mass transfer limitations, could also be a potential explanation. If that is the case, then real reaction rates are faster than observed, as they are slowed down by mass transfer, and the model assumes perfect mixing in each virtual CSTR.

### 4.7. Total Failure Experiments

A potential failure scenario identified in the risk assessment is a power failure that would cause all flow to stop. Leftover EO in the reactor can then continue to heat up the reaction mass. In a


https://doi.org/10.1021/acs.oprd.5c00362
Org. Process Res. Dev. XXXX, XXX, XXX−XXX

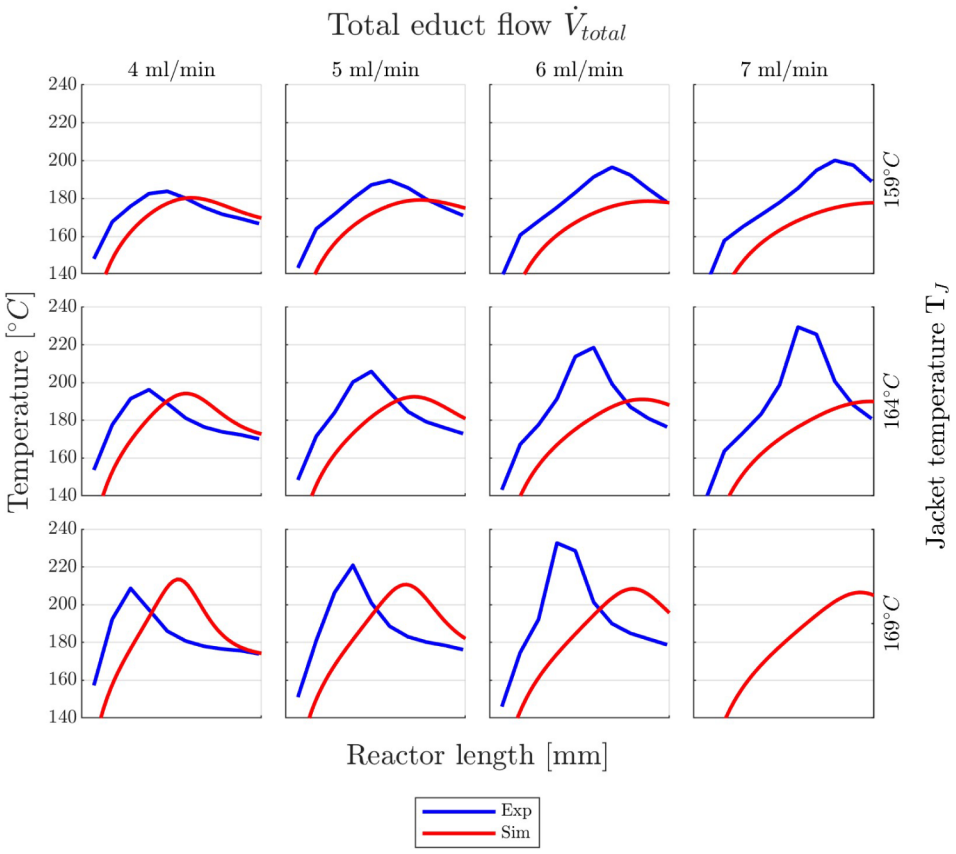


**Figure 12.** Measured (blue) and simulated (red) temperature profiles of screening experiments for 3 mequiv EO. Jacket temperatures of 159, 164, and 169 °C and total educt flow rates of 4 to 7 mL/min are screened.

standard semibatch process, insufficient cooling would lead to a thermal runaway and potential bursting of the reactor if relief or emergency cooling devices are not properly sized. In the flow process, significantly more thermal mass—static mixer, jacket wall, jacket fluid—is present in relation to accumulated reaction heat, which lowers the temperature spike. Calculation of the heat transfer in a total failure scenario is not simple, as no flow means no forced convection is present. Modeling nonforced convection in the structures of a static mixer is not trivial. Instead, a conservative model is used in this work. Under the assumption that the heat transfer between the reaction mass and the static mixer is significantly better than that to the jacket wall, we can simplify the calculation further by adding the thermal mass of the static mixer to the reaction mass. This assumption is reasonable as the relative exchange area is significantly larger. For the heat transfer, only thermal conduction in the radial direction is considered. As the jacket wall is thin and has a high thermal conductivity, its thermal resistance was neglected. Further details on the model of the total failure scenario are given in the Supporting Information. Experiments with 1.5 and 3 mequiv of EO were conducted, and the temperature profiles obtained were compared against the simulation results in Figure 13. It becomes apparent that the simple model used in this work is very conservative for a total failure scenario. The proposed model predicts a temperature rise of 60 and 104 K for 1.5 and 3 mequiv EO, respectively, while experimental data found temperature rises of only 22 and 38 K. Together with the measurements shown below, we can conclude that the FFC miniplant presented in this work can be safely operated and automatically cools down even at total failure conditions.

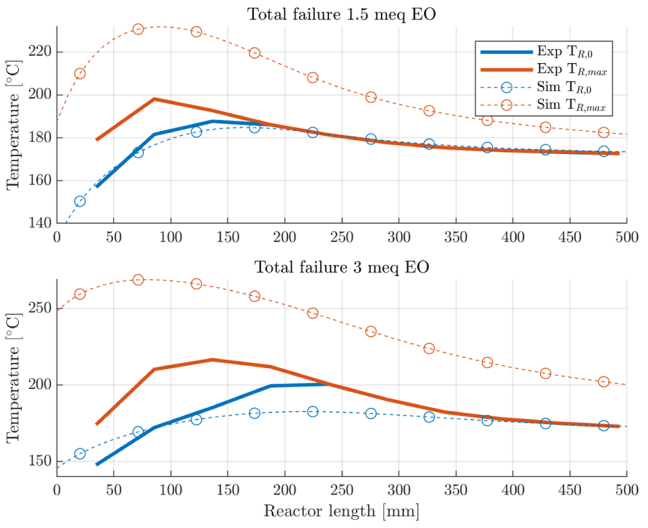


**Figure 13.** Experimental (solid) and simulated (dotted) temperature initial (blue) and maximum (orange) temperature profiles for a total failure scenario with 1.5 mequiv EO (top) and 3 mequiv EO (bottom).

## 5. CONCLUSION

Data from nonflow measurements and experiments can be used to establish an approximate flow process model, which allows the design of a flow calorimeter miniplant. Validation of



https://doi.org/10.1021/acs.oprd.5c00362
Org. Process Res. Dev. XXXX, XXX, XXX−XXX

the model components under flow conditions is critical before further scale-up is performed. As demonstrated in this work, relations and especially kinetics obtained from nonflow data may not be applicable to the extreme conditions possible in a flow process. At this time, the following parts of the model should be investigated:

- VLE: The available VLE models for EO in dodecanol were found to significantly deviate from the measured vapor pressure curves at flow conditions. Significant experimental effort is required to obtain sufficient data for model fitting. A new VLE is required to accurately predict the required back pressure and to evaluate reaction kinetics from full-batch experiments, if desired.
- Kinetics: The switch to flow allows for process conditions beyond what is possible in a semibatch process. As such, literature kinetics for semibatch processes may be inaccurate at flow conditions. In this work, the kinetics observed in flow were comparable to semibatch data for 1.5 mequiv EO. However, higher EO concentrations of 3 mequiv showed considerable, safety critical changes in behavior. As such, further kinetic studies are required under flow conditions to establish an appropriate kinetic model and fit the required parameters before further scale-up is considered.
- Temperature peak: It was found that the temperature peak increases with higher flow rates, while the model predicts an inverse relationship. This implies that an effect is not modeled, or an assumption is not holding. It is possible that local mass transfer limitations are present, which get minimized at higher flows.

A study of corrosion for long-term operations at high temperatures should be considered. While the stainless steel used in the construction of the presented miniplant is regarded as appropriate even for long-term storage of EO,[7] there is still a chance for corrosion at the high process temperatures. Coupled with the known catalytic effect of rust on EO polymerization, further studies are justified.

Overall, the value of preexisting process data in establishing a new flow process was demonstrated. However, validation under flow conditions is vital to ensure a successful scale-up, which further supports the use of miniplant flow calorimeters as a stepping stone toward manufacturing scale flow implementation. While the authors believe that the presented miniplant can be safely operated, considerable effort is still required before scale-up can be pursued.

## ■ ASSOCIATED CONTENT

### Supporting Information

The Supporting Information is available free of charge at https://pubs.acs.org/doi/10.1021/acs.oprd.5c00362.

Detailed descriptions and sources of model components (PDF)

## ■ AUTHOR INFORMATION


### Corresponding Author

**Andreas Zogg** − *Institute for Chemistry and Bioanalytics, University of Applied Sciences and Arts Northwestern Switzerland, School of Life Sciences (FHNW HLS), Muttenz 4132, Switzerland;* orcid.org/0000-0002-0053-5318; Email: andreas.zogg@fhnw.ch

### Authors

**This Zahnd** − *Institute for Chemistry and Bioanalytics, University of Applied Sciences and Arts Northwestern Switzerland, School of Life Sciences (FHNW HLS), Muttenz 4132, Switzerland*

**Benedikt Brönnimann** − *Institute for Chemistry and Bioanalytics, University of Applied Sciences and Arts Northwestern Switzerland, School of Life Sciences (FHNW HLS), Muttenz 4132, Switzerland*

**Luca Moschen** − *Institute for Chemistry and Bioanalytics, University of Applied Sciences and Arts Northwestern Switzerland, School of Life Sciences (FHNW HLS), Muttenz 4132, Switzerland*

**Corina Constantin** − *Institute for Chemistry and Bioanalytics, University of Applied Sciences and Arts Northwestern Switzerland, School of Life Sciences (FHNW HLS), Muttenz 4132, Switzerland*

**Marlies Moser** − *Fluitec Mixing + Reaction Solutions AG, Neftenbach 8413, Switzerland*

**Finn L. Steinemann** − *Fluitec Mixing + Reaction Solutions AG, Neftenbach 8413, Switzerland*

**Alain G. Georg** − *Fluitec Mixing + Reaction Solutions AG, Neftenbach 8413, Switzerland*

**Roland Borner** − *Chemische Fabrik Schärer & Schläpfer AG, Rothrist 4852, Switzerland*

Complete contact information is available at: https://pubs.acs.org/10.1021/acs.oprd.5c00362


### Author Contributions

The manuscript was written through the contributions of all authors. All authors have given approval to the final version of the manuscript.


### Funding

This work was cofunded by INNOSUISSE 101.452 IP-ENG.


### Notes

The authors declare no competing financial interest.


## ■ ACKNOWLEDGMENTS

The authors would like to thank INNOSUISSE for the financial support of this research. Over the course of this joint project between academia (FHNW), equipment manufacturer (Fluitec AG), and chemical industry (Schärer & Schläpfer AG), uncountable contributions by various people of each partner have been made. The authors would like to thank the workshop of FHNW Muttenz for their support in realizing and preparing the safety containment for the installation of the miniplant in the Process Technology Center at FHNW School of Life Sciences. Furthermore, they would like to thank Micha Hodler (Fluitec AG) for his support in the construction of the miniplant and Norbert Merkel (Fluitec AG) for building and programming the system control.


## ■ ABBREVIATIONS

EO, ethylene oxide; DSC, differential scanning Calorimeter; FFC, fluitec flow calorimeter; mequiv, molar equivalents; PFD, process flow diagram; CSTR, continuous stirred reactors; VLE, vapor−liquid equilibrium

## ■ INDICES

*i*, Component "*i*"; in, Flows into segment; init, Initiation reaction; J, Reactor jacket, Heat transfer media; *L*, Liquid



https://doi.org/10.1021/acs.oprd.5c00362
Org. Process Res. Dev. XXXX, XXX, XXX−XXX

phase of the reaction mass; out, Flows out of segment; prop, Propagation reaction; R, Index of reactor segment; RM, Reaction mass; rx, Reaction

## SYMBOLS

$A_{RJ}$, Heat exchange area [$m^2$]; $c_i$ / [$i$], Concentration of component "$i$" [mol/mL]; cp, Heat capacity [J/kg/K]; $F$, Molar flow [mol/s]; $\Delta_R H$, Heat of reaction [kJ/mol]; $k$, Kinetic constant [mL/mol/s]; $K_{ei}$, Equilibrium constant of proton transfer reaction [−]; $k_{RJ}$, Heat exchange coefficient [$W/m^2/K$]; $m$, Mass [kg]; $M$, Molar weight [g/mol]; $\dot{Q}$, Heat flow [W]; $r$, Reaction rate [mol/mL/s]; $T$, Temperature [K]; $V$, Volume [$m^3$]; $\dot{V}$, Volume flow [$m^3/s$]; $w$, Mass fraction [kg/kg]; $x$, Molar fraction [mol/mol]; $\eta$, Viscosity [Pa s]; $\lambda$, Thermal conductivity [W/m/K]

## REFERENCES


(1) Bajpai, D.; Tyagi, V. K. Nonionic Surfactants: An Overview. *Tenside, Surfactants, Deterg.* **2010**, *47* (3), 190−196.

(2) Santacesaria, E.; Tesser, R.; Di Serio, M. Polyethoxylation and Polypropoxylation Reactions: Kinetics, Mass Transfer and Industrial Reactor Design. *Chin. J. Chem. Eng.* **2018**, *26* (6), 1235−1251.

(3) Askar, E. *Experimentelle Bestimmung und Berechnung sicherheitstechnischer Kenngrößen ethylenoxidhaltiger Gasphasen*; BAM-Dissertationsreihe; Bundesanstalt für Materialforschung und -prüfung (BAM): Berlin, 2012.

(4) Ebel, H.; Hopwood, M. *Incident Investigation Report; Chemical Explosion at IQOXE in Tarragona; Incident Investigation Report 2022−9184*; 2022, 89.

(5) Mellin, B. E.*Ethylene Oxide Plant Explosion, 3 July 1987 BP Chemicals, Antwerp, Belgium*Loss Prevention Bulletin1991100

(6) *Chemical Plant Blast Heard 20 Miles Away*; Desert Sun., 1962; https://cdnc.ucr.edu/?a=d&d=DS19620417.2.14.

(7) Vogel, K.; Grumbles, T.; Jackson, S.; Lenahan, R.; Reeser, D.; Stewart, J.; Szczepanski, D.; Townsend, D.; Viscomi, R.; Wagner, M., et al. *Ethylene Oxide Product Stewardship Guidance Manual 3rd Edition*; https://www.americanchemistry.com/content/download/5642/file/Ethylene-Oxide-Product-Stewardship-Manual-3rd-Edition.pdf, (accessed 2022−09−20).

(8) Hessel, V.; Vural Gürsel, I.; Wang, Q.; Noël, T.; Lang, J. Potential Analysis of Smart Flow Processing and Micro Process Technology for Fastening Process Development: Use of Chemistry and Process Design as Intensification Fields. *Chem. Eng. Technol.* **2012**, *35* (7), 1184−1204.

(9) Noël, T.; Su, Y.; Hessel, V.Beyond Organometallic Flow Chemistry: The Principles Behind the Use of Continuous-Flow Reactors for Synthesis In *Organometallic Flow Chemistry*; Springer International Publishing: Cham, pp. 1−41, 2015; .

(10) Lebl, R.*Development Of Novel Continuous Flow Processes With Integrated Process Analytical Technology*; Dissertation(PhD), University of Graz: Graz, 2020; https://unipub.uni-graz.at/obvugrhs/content/titleinfo/5653683.

(11) Frede, T. A.; Maier, M. C.; Kockmann, N.; Gruber-Woelfler, H. Advances in Continuous Flow Calorimetry. *Org. Process Res. Dev.* **2022**, *26* (2), 267−277.

(12) Leonhardt, T.; Zogg, A.; Hutter, C.; Jeisy, J.; Riedl, W. Development of a Novel Plug-Flow System for Heterogeneously Catalyzed Multiphase Reactions. *Chem. Ing. Tech.* **2017**, *89* (4), 432−439.

(13) *Bretherick's Handbook of Reactive Chemical Hazards: an Indexed Guide to Published Data*, 7th ed., Urben, P. G., ed.; Academic: Amsterdam Boston London, 2007.

(14) Steinemann, F. L.; Rütti, D. P.; Moser, M.; Georg, A. G.; Meier, D. M. Simultaneous Determination of Enthalpy of Mixing and Reaction Using Milli-Scale Continuous Flow Calorimetry. *J. Flow Chem.* **2022**, *12* (4), 389−396.

(15) *Das PAAG-/HAZOP-Verfahren und weitere praxisbewährte Methoden: Risikobeurteilung in der Anlagensicherheit, 5. Ausgabe 3/2020.; Internationale Vereinigung für Soziale Sicherheit*; IVSS Sektion Chemie: Heidelberg, 2020.

(16) Chiu, Y.-N.*Ethoxylation Reactor Modelling And Design*; Swinburne University of Technology: Melbourne, Australia, 2005; https://researchbank.swinburne.edu.au/file/30a1ee15-6f39-4edd-b6f8-db034fbf5185/1/Yen-niChiuThesis.pdf.

(17) Amaral, G. M.; Giudici, R. Kinetics and Modeling of Fatty Alcohol Ethoxylation in an Industrial Spray Loop Reactor. *Chem. Eng. Technol.* **2011**, *34* (10), 1635−1644.

(18) Amaral, G. M.; Giudici, R. Erratum: Kinetics and Modeling of Fatty Alcohol Ethoxylation in an Industrial Spray Loop Reactor. *Chem. Eng. Technol.* **2012**, *35* (4), 598−598.

(19) *VDI-Wärmeatlas*; VDI e.V. ed.; Springer: Berlin Heidelberg, 2013, .

(20) Di Serio, M.; Tesser, R.; Felippone, F.; Santacesaria, E. Ethylene Oxide Solubility and Ethoxylation Kinetics in the Synthesis of Nonionic Surfactants. *Ind. Eng. Chem. Res.* **1995**, *34* (11), 4092−4098.

(21) Yen, L. C.; Woods, S. S. A Generalized Equation for Computer Calculation of Liquid Densities. *AIChE J.* **1966**, *12* (1), 95−99.

(22) Dever, J. P.; George, K. F.; Hoffman, W. C.; Soo, H. Ethylene Oxide. In *Kirk-Othmer Encyclopedia of Chemical Technology*; John Wiley & Sons, 2000. DOI: .

(23) Rebsdat, S.; Mayer, D. Ethylene Oxide. In *Ullmann's Encyclopedia of Industrial Chemistry*, Elvers, B.; Wiley-VCH Verlag GmbH & Co. KGaA: Weinheim, Germany, 2001; p. a10_117, DOI: .

(24) Levenspiel, O. *Chemical Reaction Engineering*; Wiley: New York Weinheim, 1998.

(25) Müller-Erlwein, E. *Chemische Reaktionstechnik*; Springer Fachmedien Wiesbaden: Wiesbaden, 2015. DOI:.

(26) Schönfeldt, N. *Surface Active Ethylene Oxide Adducts*, First English ed.; Pergamon Press: Oxford New York, 1969.

(27) Moser, M.; Georg, A. G.; Steinemann, F. L.; Rütti, D. P.; Meier, D. M. Continuous Milli-Scale Reaction Calorimeter for Direct Scale-up of Flow Chemistry. *J. Flow Chem.* **2021**, *11* (3), 691−699.

(28) Mueller, K. H.; Walters, W. D. The Thermal Decomposition of Ethylene Oxide[1,2]. *J. Am. Chem. Soc.* **1951**, *73* (4), 1458−1461.

(29) Thompson, H. W.; Meissner, M. The Kinetics of the Thermal Decomposition of Alkylene Oxides. I. Ethylene Oxide. *Trans. Faraday Soc.* **1936**, *32*, 1451.

(30) Zogg, A.; Zahnd, T.; Brönnimann, B. *Kontinuierliche Ethoxylierung*; Fachhochschule Nordwestschweiz FHNW: Muttenz, 2024; DOI: .

(31) Berufsgenossenschaft Rohstoffe und Chemische Industrie. *Reaktionen mit Ethylenoxid und andere Alkoxylierungen: Anlagensicherheit, Ausgabe 4/2022*; Heidelberg, Neckar: Anlagensicherheit; Jedermann-Verlag, 2022.

(32) Britton, L. G. Thermal Stability and Deflagration of Ethylene Oxide. *Plant/Oper. Prog.* **1990**, *9* (2), 75−86.

(33) Joshi, A.; You, X.; Barckholtz, T. A.; Wang, H. Thermal Decomposition of Ethylene Oxide: Potential Energy Surface, Master Equation Analysis, and Detailed Kinetic Modeling. *J. Phys. Chem. A* **2005**, *109* (35), 8016−8027.

(34) Chen, L.-D.; Faeth, G. M. Initiation and Properties of Decomposition Waves in Liquid Ethylene Oxide. *Combust. Flame* **1981**, *40*, 13−28.

(35) NIST. *NIST Chemistry WebBook; Gas phase thermochemistry data for Methane*; NIST Chemistry WebBook, https://webbook.nist.gov/cgi/cbook.cgi?ID=C74828&Mask=1#Thermo-Gas, (accessed 2025−04−07).

(36) NIST. *NIST Chemistry WebBook; Gas phase thermochemistry data for Ethylene oxide*; NIST Chemistry WebBook, https://webbook.nist.gov/cgi/cbook.cgi?ID=C75218&Units=SI&Mask=1#Thermo-Gas, (accessed 2025−04−07).

(37) NIST, *NIST Chemistry WebBook; Gas phase thermochemistry data for Carbon monoxide*, NIST Chemistry WebBook; https://




https://doi.org/10.1021/acs.oprd.5c00362
Org. Process Res. Dev. XXXX, XXX, XXX−XXX

webbook.nist.gov/cgi/cbook.cgi?ID=C630080&Mask=1#Thermo-Gas, (accessed 2025−04−07).
(38) Gmehling, J.; Kleiber, M.; Kolbe, B.; Rarey, J. *Chemical Thermodynamics for Process Simulation Second, completely revised and enlarged*; Wiley-VCH: Weinheim, 2019.





https://doi.org/10.1021/acs.oprd.5c00362
*Org. Process Res. Dev.* XXXX, XXX, XXX−XXX